Supporting Information

Highly Stable Lanthanide Metal-Organic Framework as an Internal Calibrated Luminescent Sensor for Glutamic Acid, a Neuropathy Biomarker

Tifeng Xia,*[,†,‡] Yating Wan,[‡] Yanping Li,[‡] and Jun Zhang*[,‡]

[†]Institute of Materials, China Academy of Engineering Physics, Mianyang 621907, P. R. China

[‡]State Key Laboratory of Silicon Materials, Cyrus Tang Center for Sensor Materials and Applications, School of Materials Science and Engineering, Zhejiang University, Hangzhou 310027, P. R. China

Corresponding Author:
xiatifeng@caep.cn;
jun-z@zju.edu.cn

Table S1. Crystallographic Data Collection and Refinement Results for ZJU-168(Eu).

	ZJU-168(Eu)
Chemical formla	$C_{48}H_{45}Eu_6O_{48}$
Formula weight	2301.60
Temperature (K)	293(2)
Wavelength (Å)	0.71073
Crystal system	Tetragonal
Space group	P4/mnc
a (Å)	15.5898(8)
b (Å)	15.5898(8)
c (Å)	21.3477(16)
V (Å^3)	5188.4(7)
Z	2
Density (calculated g/cm^3)	1.473
Absorbance coefficient (mm^{-1})	3.644
F(000)	2190
Crystal size(mm^3)	0.4X0.4X0.4
R(int)	0.1418
Goodness of fit on F_2	1.067
R_1, wR_2 [I>2σ(I)][a]	0.0446, 0.1219
R_1, wR_2 (all data)[a]	0.0639, 0.1324
Largest difference peak and hole(e/Å^3)	1.687, -1.579

$$^{a}\mathbf{R1} = \sum(|\mathbf{F_o}| - |\mathbf{F_c}|)/\sum|\mathbf{F_o}|; \mathbf{wR2} = \left[\frac{\sum \mathbf{w}(|\mathbf{F_o}| - |\mathbf{F_c}|^2)}{\sum \mathbf{wF_o^2}}\right]^{\mathbf{1/2}}$$

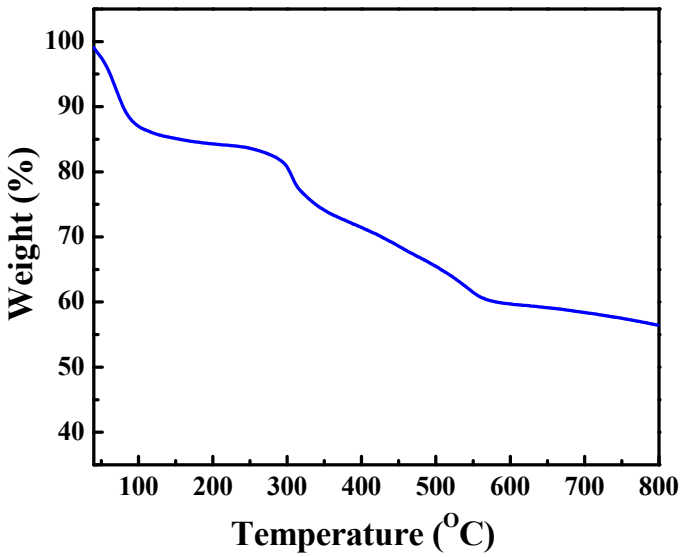

Figure S1. The TGA curve of ZJU-168(Eu).

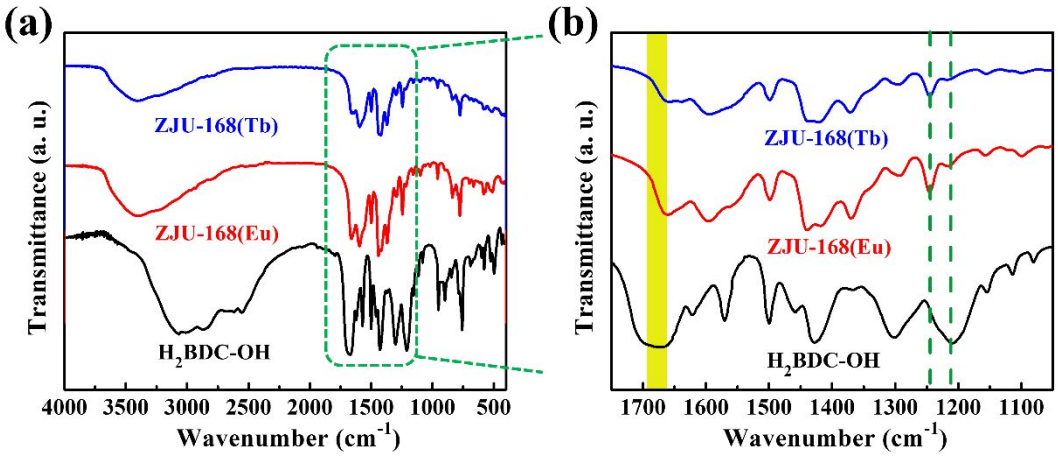

Figure S2. FI-IR spectra of H_2BDC-OH, ZJU-168(Eu) and ZJU-168(Tb).

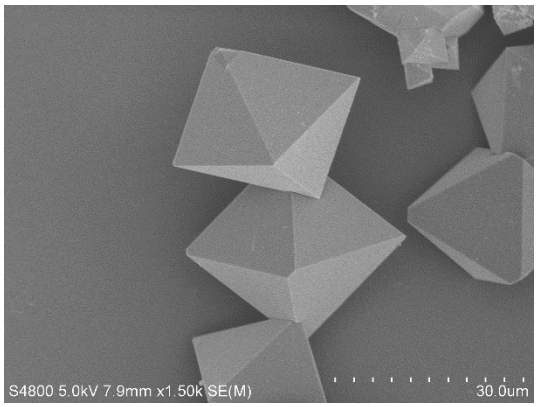

Figure S3. SEM image of ZJU-168(Eu).

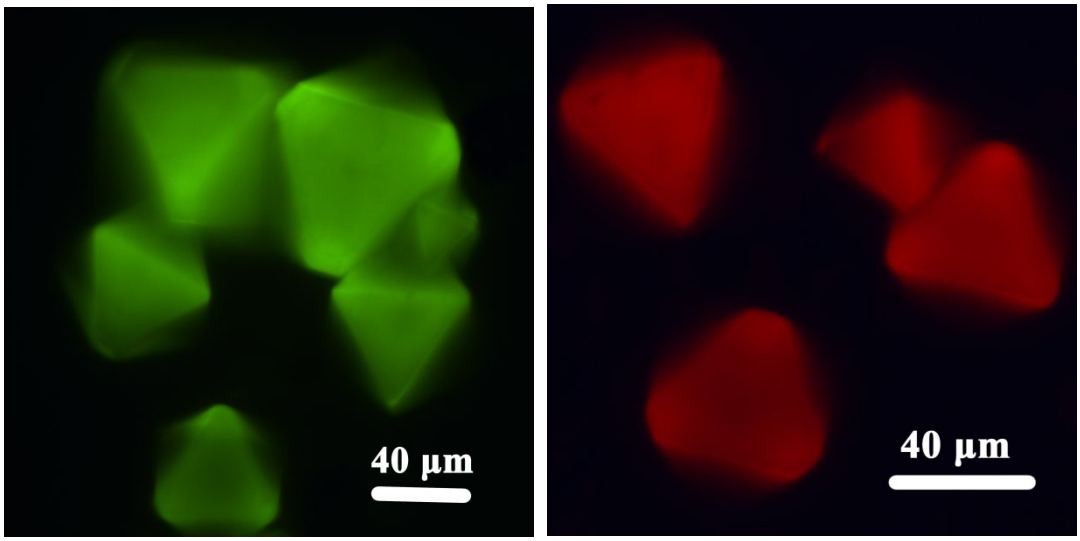

Figure S4. Micrograph of solid-state ZJU-168(Tb) (left) and ZJU-168(Eu) (right) excited by mercury lamps.

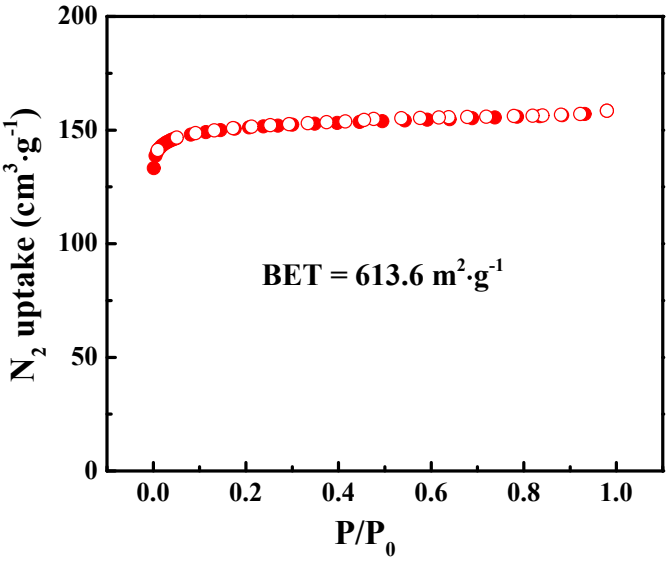

Figure S5. N_2 sorption isotherm of ZJU-168(Tb) at 77 K (solid symbols: adsorption, open symbols: desorption).

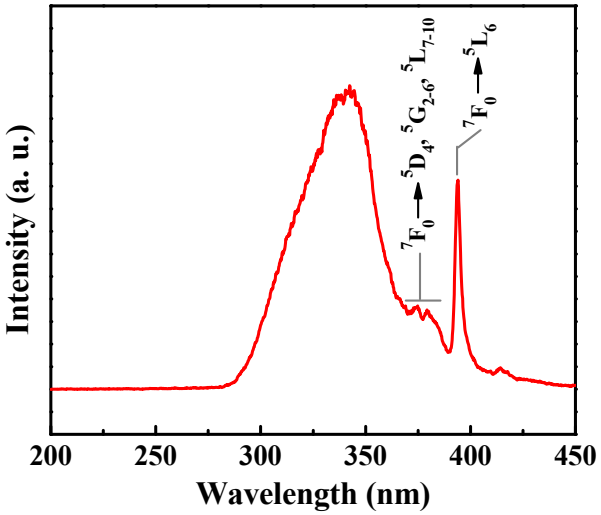

Figure S6. Excited spectrum of ZJU-168(Eu) monitored at 614 nm.

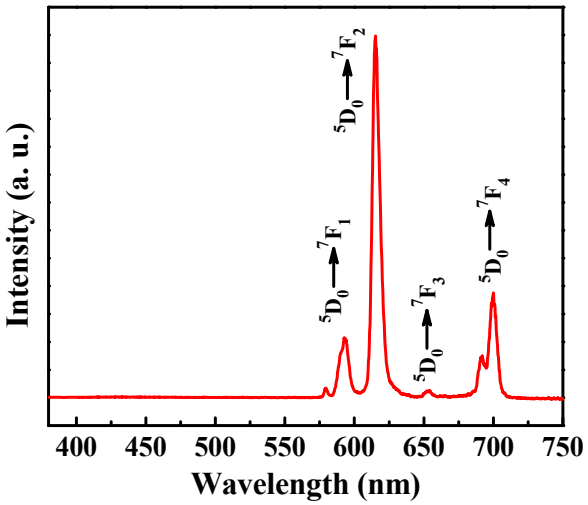

Figure S7. Emission spectrum of ZJU-168(Eu) in solid state excited at 340 nm.

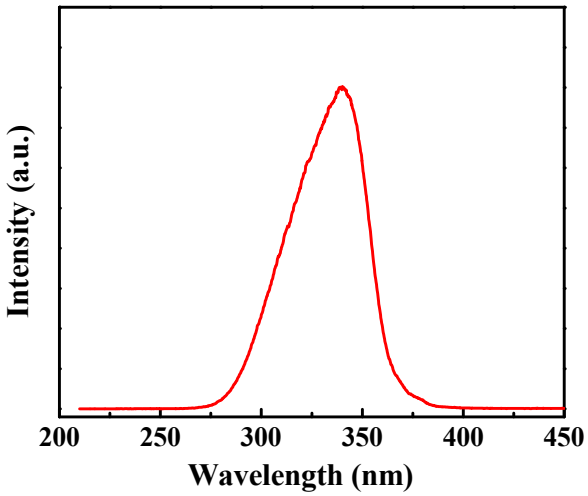

Figure S8. Excited spectrum of ZJU-168(Tb) monitored at 544 nm.

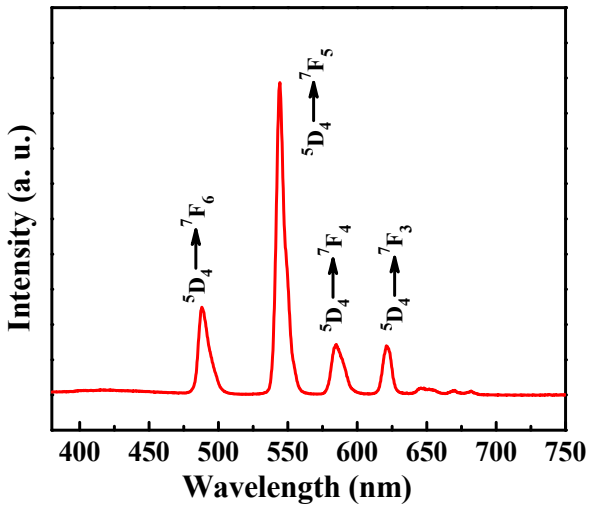

Figure S9. Emission spectrum of ZJU-168(Tb) in solid state excited at 340 nm.

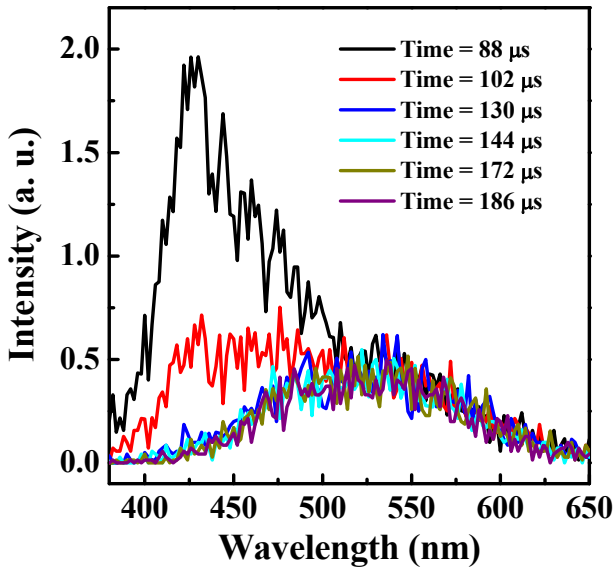

Figure S10. Time-resolved spectra of ZJU-168(Gd) at 77 K indicating the triplet state energy level of H_2BDC-OH is about 24200 cm^{-1}.

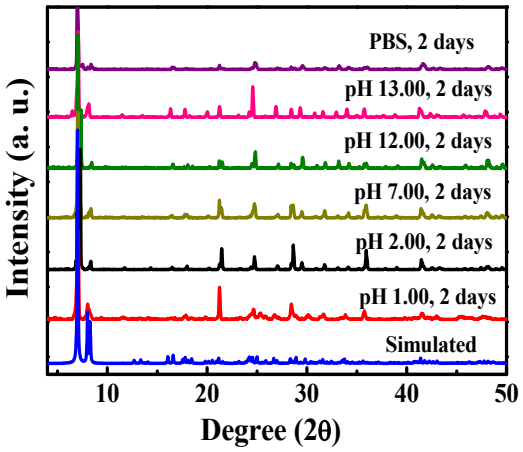

Figure S11. PXRD patterns of ZJU-168(Eu) after treatment with acid/base environment from pH 1.00 to 13.00 and phosphate buffer saline (PBS) solution for two days.

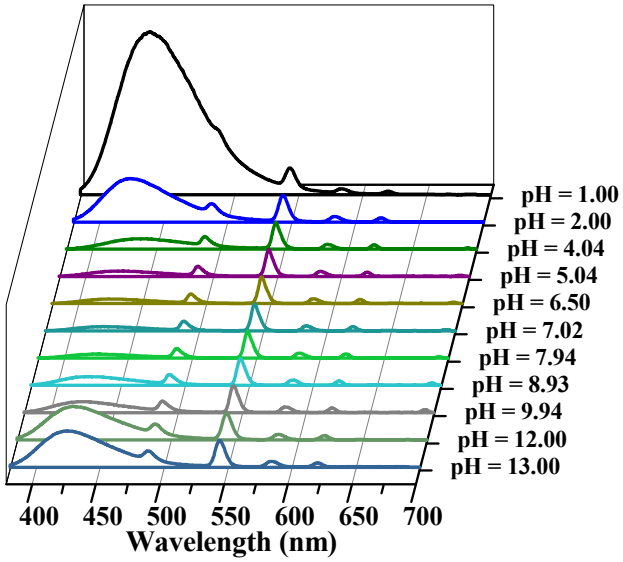

Figure S12. Luminescent emission spectra of ZJU-168(Tb) with the pH ranging from 1.00 to 13.00.

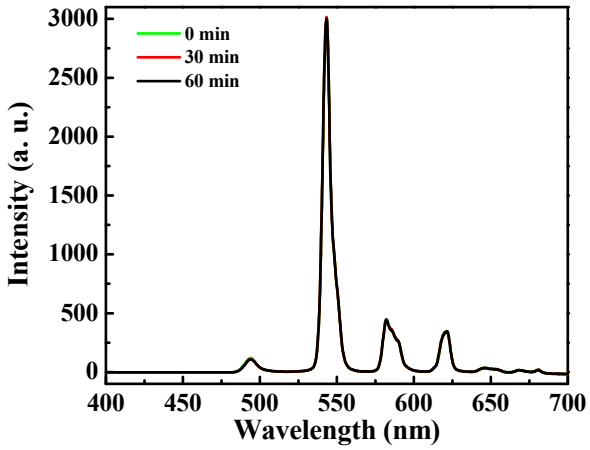

Figure S13. The photostability of ZJU-168(Tb) in solid state under continuous exposure to ultraviolet light (340 nm).

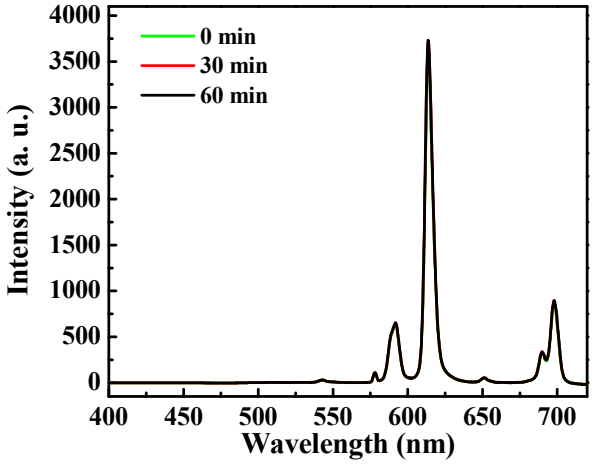

Figure S14. The photostability of ZJU-168(Eu) in solid state under continuous exposure to ultraviolet light (340 nm).

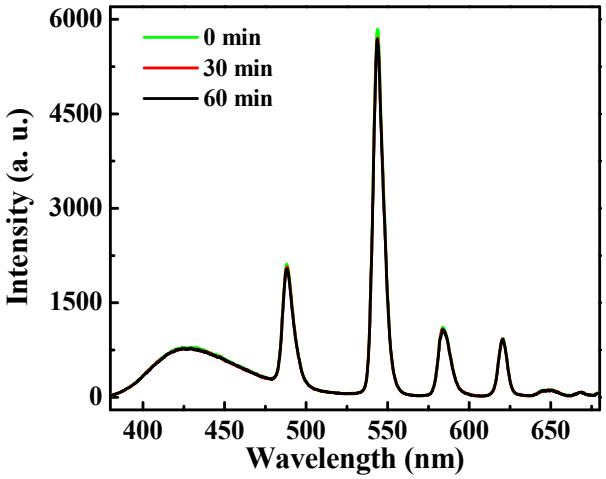

Figure S15. The photostability of aqueous suspended ZJU-168(Tb) under continuous exposure to ultraviolet light (340 nm).

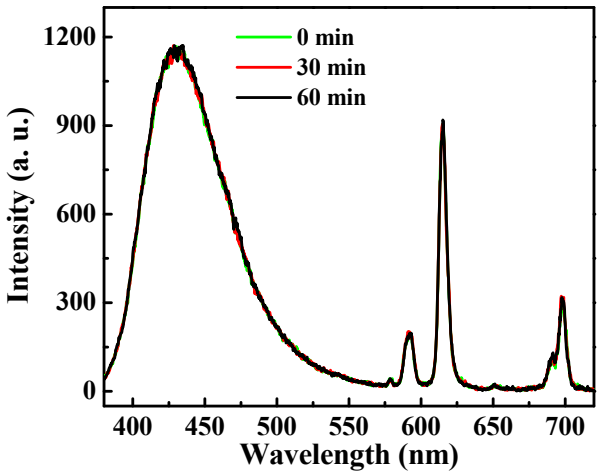

Figure S16. The photostability of aqueous suspended ZJU-168(Eu) under continuous exposure to ultraviolet light (340 nm).

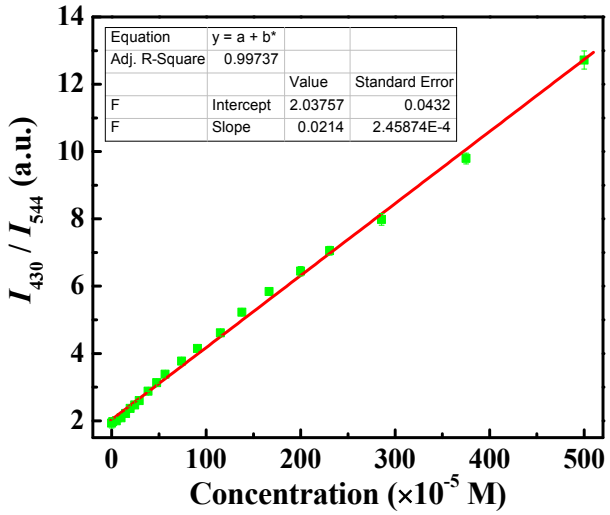

Figure S17. Integrated luminescence intensity ratios (I_{430}/I_{544}) of ZJU-168(Tb) versus Glu concentration and the fitting line.

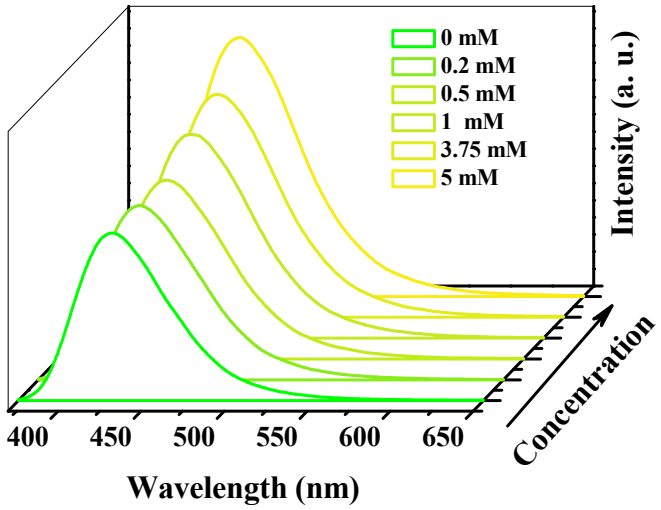

Figure S18. Luminescent emission spectra of ZJU-168(Gd) with the increase of Glu from 0 mM to 5 mM.

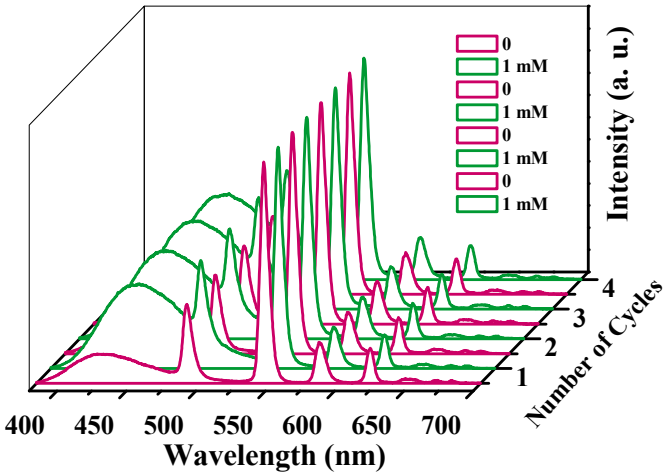

Figure S19. Recyclability test of ZJU-168(Tb) by alternately exposed to aqueous solutions with different Glu concentration (0 mM and 1 mM).

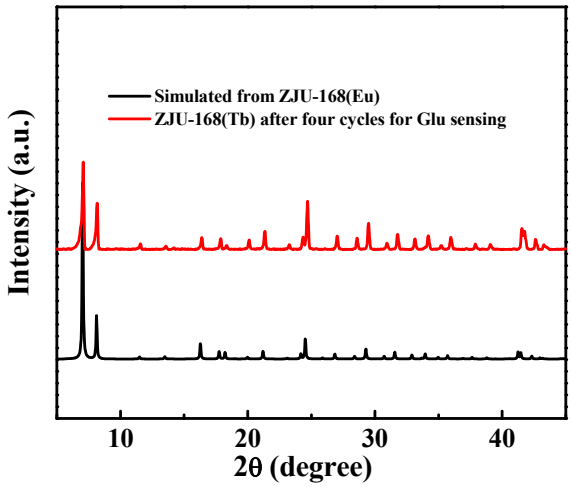

Figure S20. PXRD of ZJU-168(Tb) after four consecutive cycles for Glu sensing.

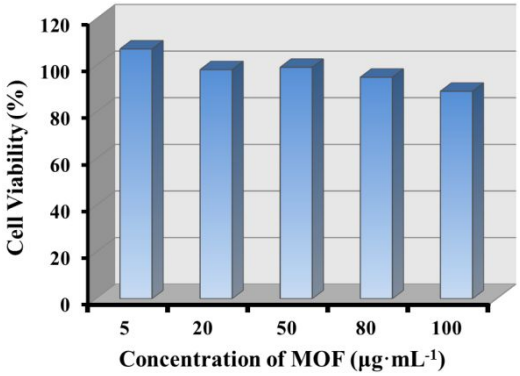

Figure S21. Cell viability data of ZJU-168(Tb) obtained from cultured PC12 cells.

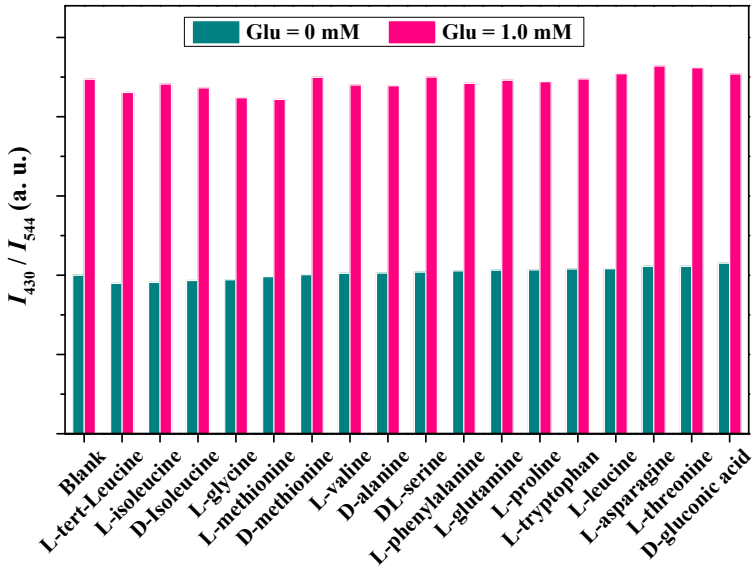

Figure S22. Selectivity of ZJU-168(Tb) to Glu in the presence of other amino acids. The dark cyan and pink columns represent the absence and presence of Glu, respectively.

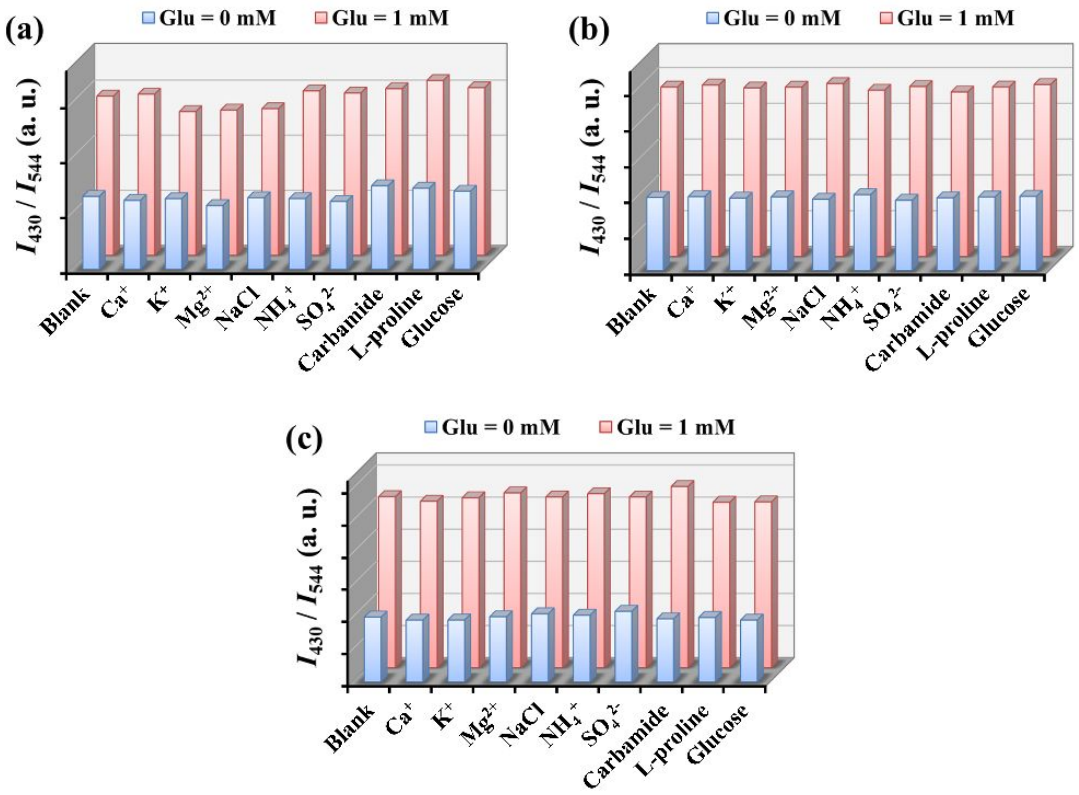

Figure S23. Selectivity of ZJU-168(Tb) to Glu in (a) pH 5.4, (b) pH 6.8, (c) pH 7.4 solutions. The dark red and dark blue columns represent the absence and presence of Glu, respectively.

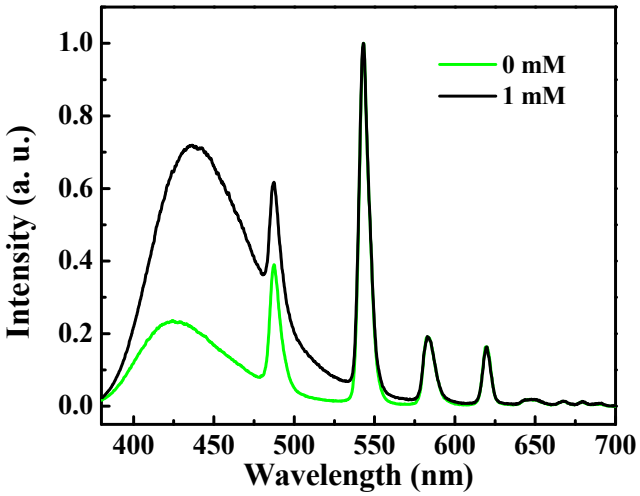

Figure S24. Luminescent emission spectra of ZJU-168(Tb) with the absence and presence of Glu in the dilute fetal bovine serum.

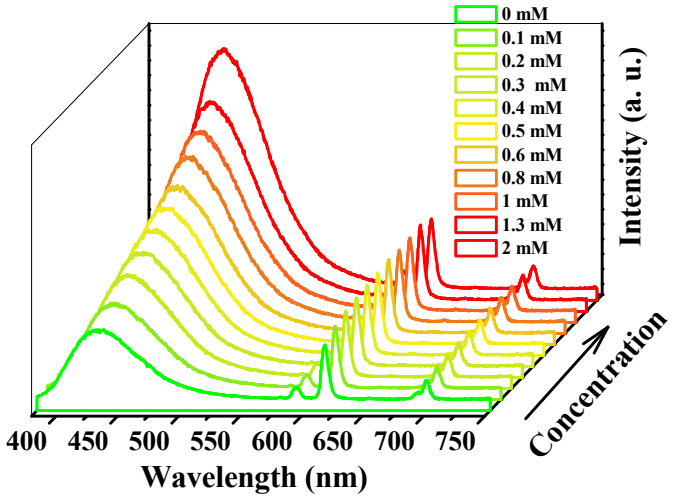

Figure S25. Luminescent emission spectra of ZJU-168(Eu) with the increase of Glu from 0 mM to 2 mM.

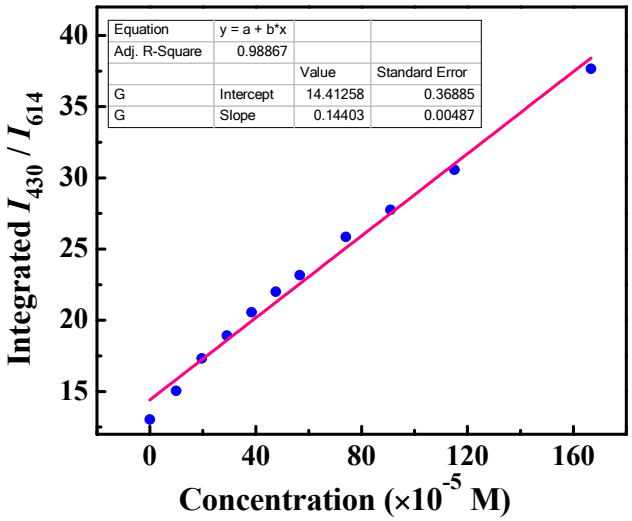

Figure S26. Integrated luminescence intensity ratio of ZJU-168(Eu) versus Glu concentration and the fitting line.

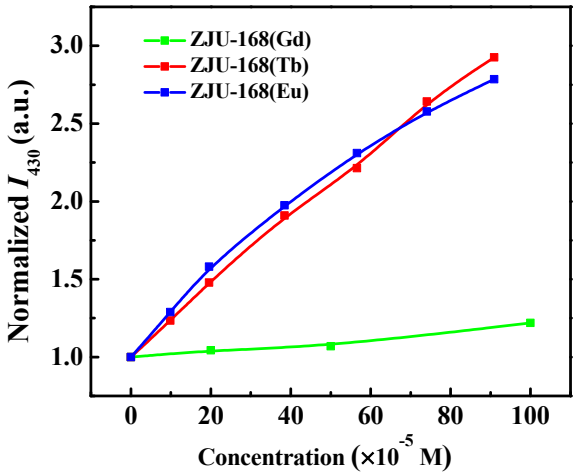

Figure S27. The normalized ligand emission of ZJU-168(Tb), ZJU-168(Eu) and ZJU-168(Gd) versus Glu concentration.

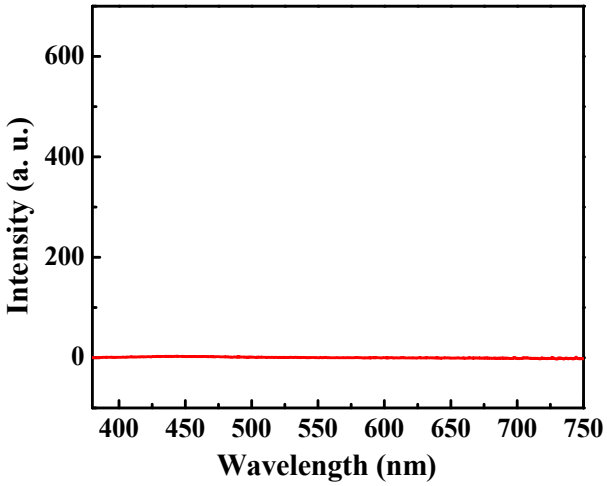

Figure S28. Emission spectrum of Glu aqueous (0.01 mol·L^{-1}) excited at 340 nm.

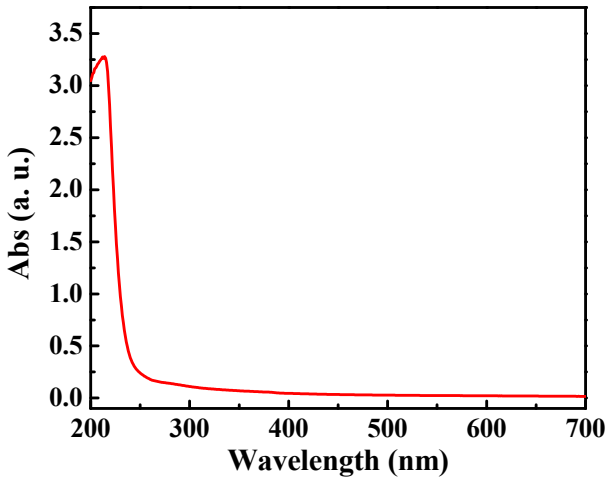

Figure S29. Absorption spectrum of Glu aqueous (0.01 mol·L^{-1}).

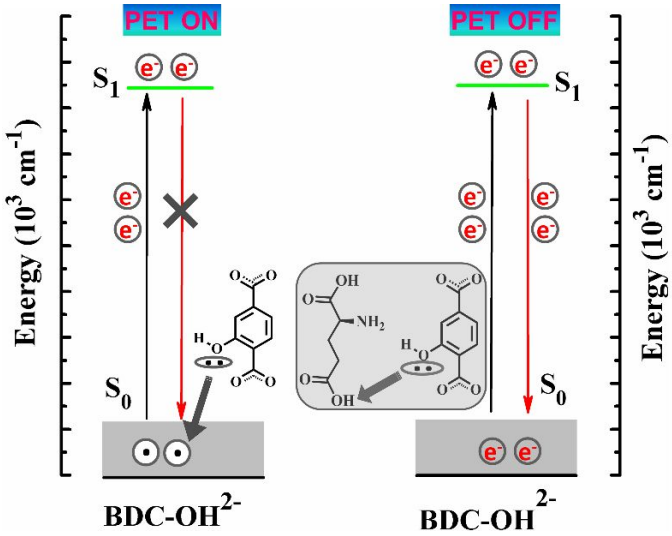

Figure S30. The possible mechanism for the self-calibrated detection of Glu by ZJU-168(Tb). The interaction between Glu and hydroxyl inhibits PET process, leading to the enhancement of ligand emission. However, T_1 of ligand doesn't change, so the emission from Tb^{3+} is almost unchanged.

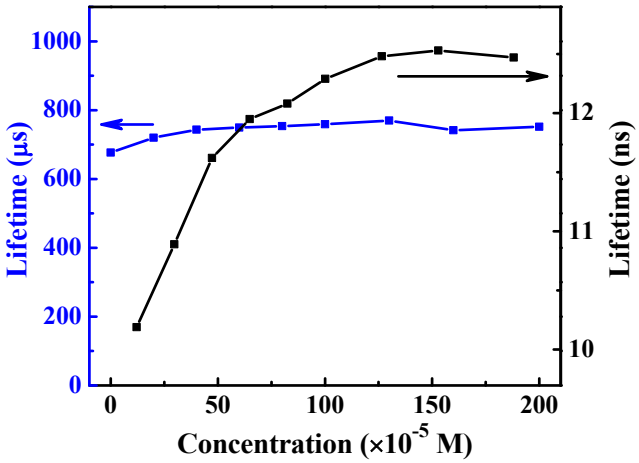

Figure S31. Luminescence lifetimes of ZJU-168(Tb) towards various Glu concentrations in aqueous solution (black: ligand; blue: Tb^{3+}).